High/low-moment phase transition in hexagonal Mn-Fe-P-Si compounds

N. H. Dung,[1,*] L. Zhang,[1,2] Z. Q. Ou,[1] L. Zhao,[3] L. van Eijck,[4] A. M. Mulders,[5] M. Avdeev,[6] E. Suard,[7] N. H. van Dijk,[1] and Ekkes Brück[1]

[1]*Fundamental Aspects of Materials and Energy, Faculty of Applied Sciences, Delft University of Technology, Mekelweg 15, 2629 JB Delft, Netherlands*

[2]*BASF Nederland B.V., Strijkviertel 67, 3454 PK De Meern, Netherlands*

[3]*Department of Materials Science and Engineering, Delft University of Technology, Mekelweg 2, 2628 CD Delft, Netherlands*

[4]*Neutron and Positron Methods in Materials, Faculty of Applied Sciences, Delft University of Technology, Mekelweg 15, 2629 JB Delft, Netherlands*

[5]*The University of New South Wales in Canberra, Canberra, Australian Capital Territory 2600, Australia*

[6]*Bragg Institute, Australian Nuclear Science and Technology Organization (ANSTO), Kirrawee DC NSW 2232, Australia*

[7]*Institut Laue Langevin (ILL), F-38042 Grenoble, France*

(Received 23 September 2011; published 27 July 2012)

Using high-resolution neutron diffraction measurements for Mn-rich hexagonal Mn-Fe-P-Si compounds, we show that the substitution of Mn for Fe on the $3f$ sites results in a linear decrease of the Fe/Mn($3f$) magnetic moments, while the Mn($3g$) magnetic moments remain constant. With increasing temperature, the Mn($3g$) magnetic moments show almost no change, while the Fe/Mn($3f$) moments decrease quickly when the transition temperature is approached. The reduction of the magnetic moments at the transition temperature and in the high-temperature range is discussed based on changes in interatomic distances and lattice parameters and high-temperature magnetic-susceptibility measurement.

DOI: 10.1103/PhysRevB.86.045134 PACS number(s): 75.30.Sg, 64.70.kd, 75.30.Kz, 75.50.Bb

I. INTRODUCTION

The interplay between crystal structure and magnetism, which is often very pronounced in first-order magnetic transition (FOMT) materials, is proposed to be at the core of giant magnetocaloric effect (MCE). Up to now, giant MCE has been discovered in several materials which are promising for room-temperature magnetic refrigeration applications.[1–7] Although a magnetic phase transition coupled with a change in crystal structure can be observed clearly in these materials, pinpointing the microscopic mechanism for the coupling between magnetism and crystal structure is not easy. By using x-ray magnetic circular dichroism and density functional theory, the mechanism of first-order bond-breaking magneto-structural transition in $Gd_5Ge_{4-x}Si_x$ was clarified with emphasis on the role of Ge in bridging ferromagnetism.[8] Spin-dependent hybridization between Ge $4p$ and Gd $5d$ conduction states enables long-range Ruderman–Kittel–Kasuya–Yosida (RKKY) ferromagnetic interactions between Gd $4f$ moments in adjacent Gd slabs connected by Ge/Si-Ge/Si bonds. Hence, ferromagnetic order will be destroyed if the RKKY interactions are weakened above the Ge/Si-Ge/Si bond-breaking transition. The chemical bonding between Ge/Si atoms plays an important role in first-order magneto-structural transition for this class of materials. For $LaFe_{13-x}Si_x$, electronic structure calculations indicated the existence of several shallow minima and maxima in the total energy vs the spin-moment curve, resulting in a ferro- to paramagnetic transition that involves a series of consecutive transitions.[9] The extremes in the theoretical total energy profile are very sensitive to the lattice parameter of the cubic $LaFe_{13-x}Si_x$ phase. Although a peculiar series of consecutive field-induced transitions were realized in $La(Fe,Si)_{13}H_x$ under pressure,[10] a microscopic mechanism is still lacking for the FOMT in this class of materials. Similarly, for $Ni_{0.50}Mn_{0.50-x}Sn_x$ with an inverse MCE, the FOMT is often ascribed to a change in atomic distance at the martensitic transition that modifies magnetic properties of the alloy.[5] However, *ab initio* electronic structure calculations still need to be done for a microscopic interpretation of the FOMT.[5]

First-principle electronic-structure calculations for hexagonal MnFe(P,Si) revealed the coexistence of strong and weak magnetism in alternate atomic layers.[7] These atomic layers are formed by the preferential occupation of Mn and Fe on the $3g$ and $3f$ sites, respectively. While the magnetic transition only causes a small reduction in the Mn moments on the $3g$ sites, the disappearance of the Fe moments in the paramagnetic state demonstrates that there is a strong coupling between magnetism and crystal lattice. The competition between chemical bonding and moments is proposed to be at the basis of the FOMT. Therefore, a detailed study of the magnetic moments on different sites is needed to clarify the origin of the first-order magneto-elastic transition.

In this paper, we focus on the determination of the magnetic structure and magnetic moments using neutron diffraction measurements on Mn-rich hexagonal $Mn_xFe_{1.95-x}P_{0.50}Si_{0.50}$ compounds ($x > 1.0$) with special attention paid to compounds ($x < 1.4$) displaying a first-order magneto-elastic transition.[11] The reduction of the moment caused by the first-order magneto-elastic transition is discussed based on a sudden change in the interatomic distances at the transition temperature (T_C), an anomalous thermal expansion of the lattice parameters in the paramagnetic state and high-temperature magnetic-susceptibility measurement.

II. EXPERIMENTAL DETAILS

The Mn-rich $Mn_xFe_{1.95-x}P_{0.50}Si_{0.50}$ compounds were prepared as described in Ref. 11. To make the samples more homogeneous, they were reannealed at 1373 K for 20 h before being

quenched in cold water. A superconducting quantum interference device (SQUID) magnetometer (Quantum Design MPMS 5XL) with the reciprocating sample option (RSO) mode was employed for magnetic measurements below 400 K. High-temperature magnetic measurements were carried out using a vibrating sample magnetometer (VSM; model LakeShore 7307) with a high-temperature oven (model 73034). The neutron diffraction data were collected at the Bragg Institute of the Australian Nuclear Science and Technology Organization (ANSTO) on the ECHIDNA high-resolution powder diffractometer[12] with an incident wavelength of 1.622 Å for the $x = 1.20$, 1.25, and 1.30 samples, and at the Institut Laue-Langevin (ILL) on the D2B high-resolution powder diffractometer[13] with an incident wavelength of 1.595 Å for the $x = 1.95$ sample. The sample powder was contained in a vanadium can which is mounted in a cryostat. The measurements were carried out at fixed temperatures from 5 to 400 K in zero field. The x-ray diffraction patterns were collected at various temperatures in zero field using a PANalytical X-pert Pro diffractometer equipped with an Anton Paar TTK450 low-temperature chamber using Cu Kα radiation, a secondary-beam flat-crystal monochromator and a multichannel X'celerator detector. Starting at 150 K, each x-ray pattern was recorded at a constant temperature, and the following one was recorded at a higher temperature, up to 500 K.

III. RESULTS AND DISCUSSION

All the samples studied display a para- to ferromagnetic transition. Figure 1(a) shows the neutron diffraction patterns for the $x = 1.30$ sample at 285 K in the paramagnetic state and 5 K in the ferromagnetic state. The Rietveld refinement carried out using the FullProf program[14] confirms hexagonal Fe_2P-type of structure (space group P-62m). The results listed in Table I show that Mn prefers the 3g sites, while Fe favors the 3f sites. In the Mn-rich compounds, some Mn will occupy the 3f sites (see Fig. 2). The refinement also indicates that P and Si are randomly distributed on the 2c and 1b sites. Earlier studies on MnFe(P,Si) have pointed out that the magnetic moments prefer to be in the ab plane rather than in the c direction, as observed in Fe_2P.[15,16] In the present study, the low-temperature diffraction pattern fits well when the magnetic moments are aligned in the ab plane, indicating that replacing some Fe with Mn on the 3f sites does not affect the preferential alignment of the magnetic moments.

Recently, we have shown that, for the Mn-rich $Mn_xFe_{1.95-x}P_{0.50}Si_{0.50}$ compounds with increasing Mn/Fe ratios, the first-order magneto-elastic transition ($x < 1.40$) changes into a first-order magneto-structural transition via a second-order isostructural magnetic transition ($x \geqslant 1.40$).[11] However, the hexagonal structure is stable in the ferromagnetic state at low temperature for all Mn/Fe ratios. By using neutron diffraction, we find that the alignment of the magnetic moments in the ab plane is also maintained until Fe is completely replaced by Mn on the 3f sites [see Fig. 1(b) and Table I]. Interestingly, the Mn(3g) moments remain constant at about 2.6 μ_B, while the Fe/Mn(3f) moments decrease linearly from 1.5 μ_B for $x = 1.20$ down to 0.4 μ_B for $x = 1.95$ (see Fig. 3). The total moments obtained from macroscopic measurements of the low-temperature saturation

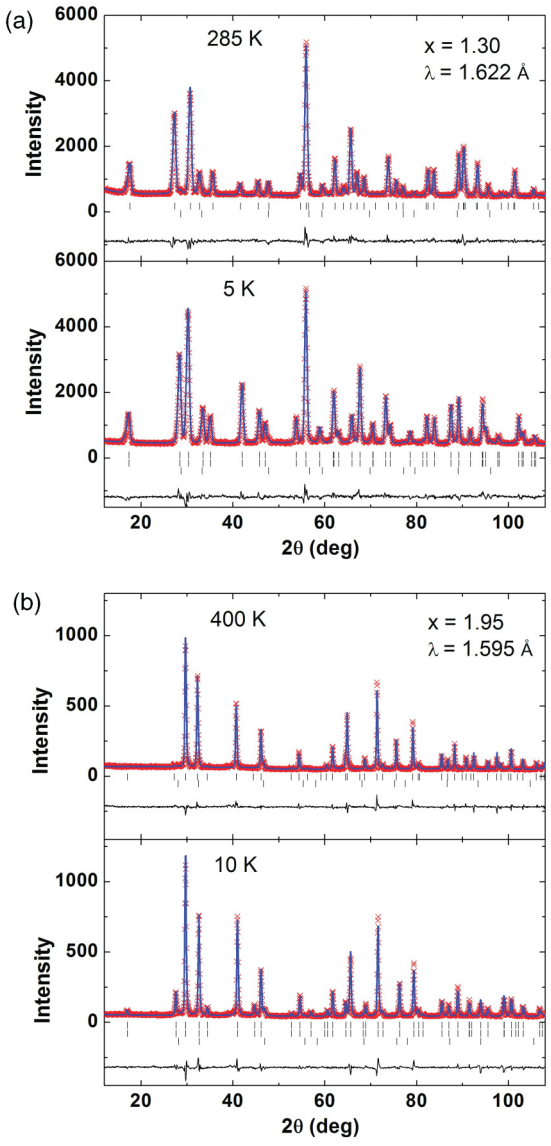

FIG. 1. (Color online) Observed (crosses), calculated (continuous lines) neutron diffraction patterns for hexagonal (a) $Mn_{1.30}Fe_{0.65}P_{0.50}Si_{0.50}$ ($\lambda = 1.622$ Å) and (b) $Mn_{1.95}P_{0.50}Si_{0.50}$ ($\lambda = 1.595$ Å) in the para- (upper plot) and ferromagnetic (lower plot) state. Differences are shown in the low part of the plots. The low-temperature diffraction patterns were fitted with the magnetic moments aligned in the ab plane. The refined parameters are listed in Table I. A very small amount of cubic $(Mn,Fe)_3Si$ impurity phase is detected. Vertical lines indicate the diffraction peaks for the nuclear (top) and magnetic (middle, if any) structure of the main phase, and the impurity phase $(Mn,Fe)_3Si$ (bottom).

magnetization are very close to those derived from the neutron diffraction patterns at 3–10 K. The linear reduction of the Fe/Mn(3f) moments for increasing x indicates that the Mn atom may develop a much lower magnetic moment than the Fe atom on the 3f sites.

To investigate the thermal evolutions of the magnetic and structural properties, neutron diffraction measurements were performed at different temperatures for the $x = 1.25$ sample exhibiting a first-order magneto-elastic transition. At 280 K, coexistence of the ferro- and paramagnetic phases was detected

TABLE I. Structural parameters of hexagonal $Mn_{1.30}Fe_{0.65}P_{0.50}Si_{0.50}$ and $Mn_{1.95}P_{0.50}Si_{0.50}$ in the paramagnetic and ferromagnetic state. Group space: P-62m. Atomic positions: 3g (x_1,0,1/2); 3f (x_2,0,0); 2c (1/3,2/3,0); and 1b (0,0,1/2). These parameters are derived from neutron diffraction patterns in Fig. 1.

		$x = 1.30$		$x = 1.95$	
Refined parameters		285 K Paramagnetic	5 K Ferromagnetic	400 K Paramagnetic	10 K Ferromagnetic
Unit cell	a (Å)	6.11390(4)	6.20611(4)	6.21889(4)	6.2145(1)
	c (Å)	3.42997(4)	3.29842(4)	3.38478(3)	3.3400(1)
	V (Å^3)	111.034(2)	110.021(2)	113.367(1)	111.709(4)
3g	x_1	0.5918(3)	0.5971(3)	0.5948(3)	0.5968(3)
	n(Mn)/n(Fe)	0.249/0.001(1)	0.249/0.001(1)	0.25/0	0.25/0
	B (Å^2)	0.83(4)	0.44(3)	0.89(4)	0.11(3)
	M (μ_B)		2.74(4)		2.61(3)
3f	x_2	0.2562(2)	0.2585(2)	0.2531(4)	0.2531(4)
	n(Fe)/n(Mn)	0.168/0.082(1)	0.168/0.082(1)	0/0.25	0/0.25
	B (Å^2)	0.81(3)	0.48(2)	1.14(3)	0.35(3)
	M (μ_B)		1.20(4)		0.36(3)
2c	n(P)/n(Si)	0.066/0.101(2)	0.066/0.101(2)	0.064/0.103(6)	0.064/0.103(6)
	B (Å^2)	0.39(4)	0.42(4)	0.59(5)	0.05(3)
1b	n(P)/n(Si)	0.059/0.024(2)	0.059/0.024(2)	0.061/0.022(6)	0.061/0.022(6)
	B (Å^2)	0.85(6)	0.53(4)	1.21(8)	0.30(4)
	Rp (%)	3.75	4.27	5.61	6.19
	wRp (%)	4.92	5.52	7.31	7.99
	χ^2	3.42	4.16	4.15	4.99

(see Fig. 4). The fraction of the ferro- to paramagnetic phase is estimated to be 33:67. While the Mn(3g) moments show almost no change for increasing temperature, the Fe/Mn(3f) moments rapidly decrease near T_C (see Fig. 5). This behavior is similar to that observed for $Mn_{1.1}Fe_{0.9}P_{0.8}Ge_{0.2}$ by Liu *et al.*[17] This may be the signature for the reduction of magnetic moments, especially on the 3f sites, at T_C which we proposed based on theoretical calculations.[7]

Figure 6 illustrates the temperature dependence of the lattice parameters and the distances between the magnetic atoms and the nearest neighbors for the $x = 1.25$ sample. At temperatures below T_C, the lattice parameters change in the opposite sense, i.e. the a parameter decreases, while the c

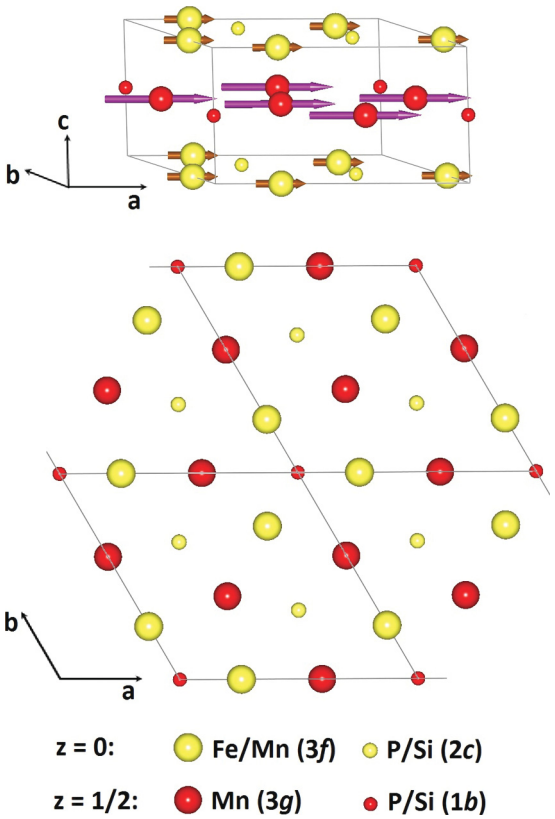

FIG. 2. (Color online) Atomic and spin arrangement within the unit cell of the Mn-rich $(Mn,Fe)_2(P,Si)$ compounds.

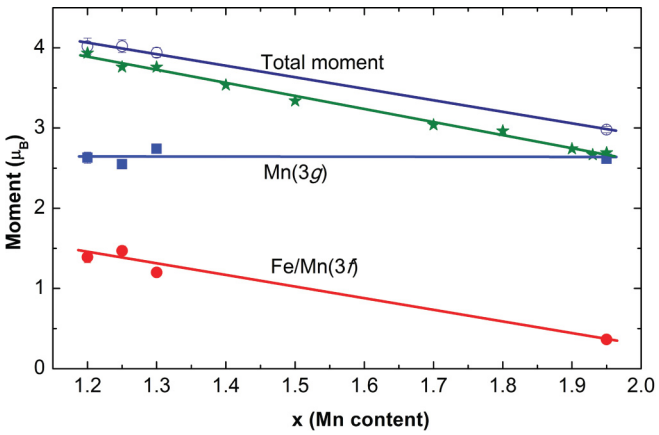

FIG. 3. (Color online) Composition dependence of the magnetic moments derived from the neutron diffraction patterns measured at 3–10 K for $Mn_xFe_{1.95-x}P_{0.50}Si_{0.50}$. The total magnetic moments per formula unit (empty circles) are very close to those obtained from saturation magnetization measurements at 5 K (solid stars).

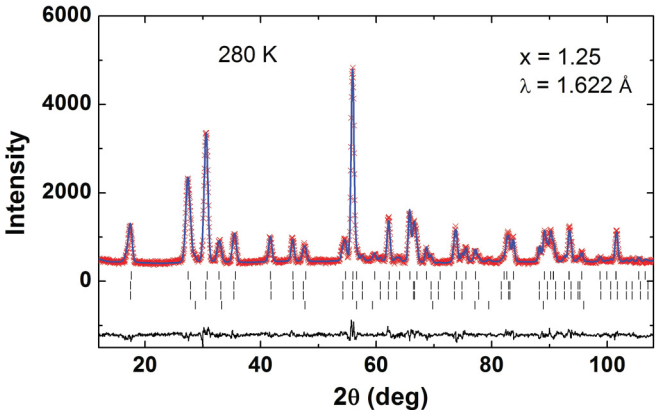

FIG. 4. (Color online) Observed (crosses) and calculated (continuous lines) neutron diffraction patterns for $Mn_{1.25}Fe_{0.70}P_{0.50}Si_{0.50}$ ($\lambda = 1.622$ Å) at 280 K at which the ferro- and paramagnetic phases are coexistent. The lattice parameters and interatomic distances between the magnetic atoms and their nearest neighbors are listed in Table II. From top to bottom, vertical lines indicate the diffraction peaks for the nuclear structure of the paramagnetic phase, the nuclear and magnetic structure of the ferromagnetic phase, and the impurity phase $(Mn,Fe)_3Si$.

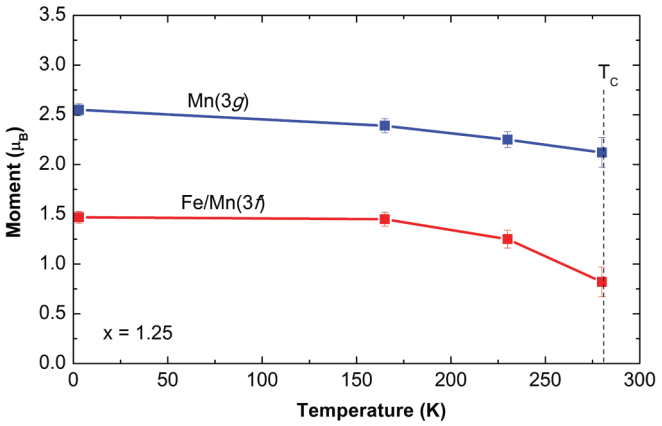

FIG. 5. (Color online) Ordered magnetic moments as a function of temperature derived from neutron diffraction patterns measured at fixed temperatures upon heating for $Mn_{1.25}Fe_{0.70}P_{0.50}Si_{0.50}$.

parameter increases with increasing temperature. This happens gradually near and below T_C and abruptly at the transition. The interatomic distances of the ferro- and paramagnetic phases at T_C are listed in Table II. The mean Mn(3*g*)-P/Si and Fe/Mn(3*f*)-P/Si distances show almost no change at the transition temperature, while sudden changes in the mean distances between the magnetic atoms are observed. It should be noted that the distances between the intralayer magnetic atoms drop strongly, enhancing the overlap between the 3*d* states and resulting in an abrupt reduction of the magnetic moments. However, the relative displacement of the Mn(3*g*) atoms during the transition is smaller than that of the Fe/Mn(3*f*) atoms. Furthermore, the intralayer Mn(3*g*)-Mn(3*g*) distance is larger than the intralayer Fe/Mn(3*f*)-Fe/Mn(3*f*) distance, and the Mn 3*d* electrons are more localized. Thus, the reduction of the Mn(3*g*) moments is much smaller than that of the Fe/Mn(3*f*) moments. In terms of mean distances, the reduction of the distances between the intralayer magnetic atoms makes the main contribution to the decrease in the magnetic moments, especially for the Fe/Mn(3*f*) layers. This may be a common feature for all other hexagonal Fe_2P-based materials exhibiting a first-order magneto-elastic transition.[17] The above arguments confirm

TABLE II. Lattice parameters and interatomic distances of $Mn_{1.25}Fe_{0.70}P_{0.50}Si_{0.50}$ at 280 K at which the ferro- and paramagnetic phases are coexistent. These data are derived from neutron diffraction pattern in Fig. 4.

			280 K	
			Ferromagnetic	Paramagnetic
Lattice parameters				
a (Å)			6.1638(1)	6.1163(1)
c (Å)			3.3653(1)	3.4212(1)
V (Å^3)			110.726(4)	110.837(3)
Interatomic distances: Mn(3*g*)-nearest neighbors (Å)				
Mn(3*g*)-Mn(3*g*)	Intralayer	× 4	3.242(6)	3.196(4)
Mn(3*g*)-Fe/Mn(3*f*)	Interlayer	× 1	2.670(7)	2.660(3)
	Interlayer	× 2	2.764(6)	2.790(3)
	Mean distance		2.733(4)	2.747(2)
Mn(3*g*)-P/Si	Interlayer	× 4	2.517(3)	2.516(3)
	Intralayer	× 1	2.501(6)	2.522(4)
	Mean distance		2.514(2)	2.517(1)
Interatomic distances: Fe/Mn(3*f*)-nearest neighbors (Å)				
Fe/Mn(3*f*)-Fe/Mn(3*f*)	Intralayer	× 2	2.753(6)	2.696(3)
Fe/Mn(3*f*)-Mn(3*g*)	Interlayer	× 1	2.670(7)	2.660(3)
	Interlayer	× 2	2.764(6)	2.790(3)
	Mean distance		2.733(4)	2.747(2)
Fe/Mn(3*f*)-P/Si	Intralayer	× 2	2.322(3)	2.318(2)
	Interlayer	× 2	2.315(3)	2.313(2)
	Mean distance		2.319(2)	2.316(1)

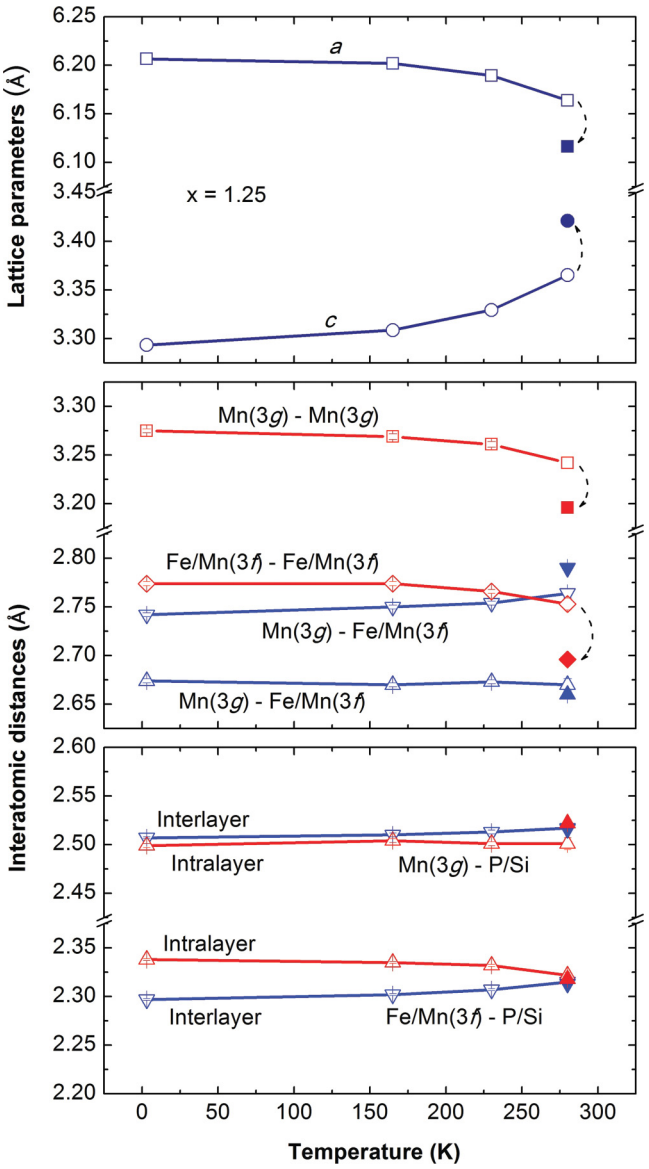

FIG. 6. (Color online) Lattice parameters and interatomic distances as a function of temperature derived from neutron diffraction patterns measured at fixed temperatures upon heating for $Mn_{1.25}Fe_{0.70}P_{0.50}Si_{0.50}$ in the ferromagnetic (empty symbols) and paramagnetic (solid symbols) state.

our proposal for the competition between chemical bonding and moments. The observed behaviors of the moments and the lattice parameter below T_C indicate that the competition between chemical bonding and moments becomes stronger when T_C is approached.

The value of the lattice parameters obtained from the neutron diffraction measurements is in good agreement with that derived from x-ray diffraction patterns by using the FullProf refinement program (see Fig. 7). It should be noted that, above T_C, we observe nonlinear temperature variations of the lattice parameters up to a certain temperature T_O, while the volume increases linearly with temperature. It seems that the competition between chemical bonding and moments does not affect the volume because there is only a small volume change of about 0.1 % at T_C, and a linear variation of the volume

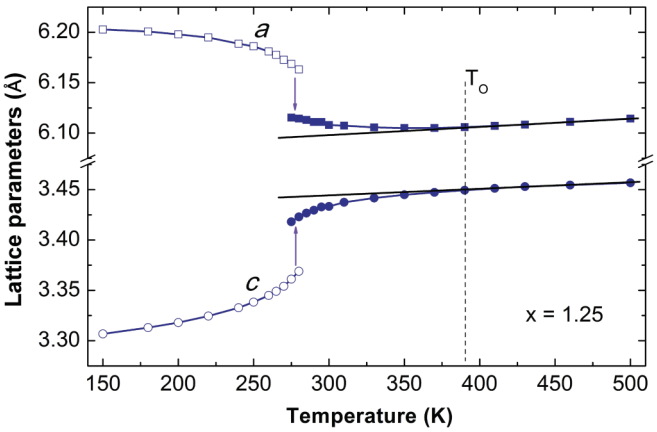

FIG. 7. (Color online) Lattice parameters as a function of temperature derived from x-ray diffraction patterns measured at fixed temperatures upon heating for $Mn_{1.25}Fe_{0.70}P_{0.50}Si_{0.50}$. The error bar is smaller than the size of the symbols.

is also observed at temperatures well below T_C. The value of T_O is determined to be about 390 K for the $x = 1.25$ sample. The nonlinear variations of the lattice parameters imply that the competition between chemical bonding and moments still continues above T_C. Thus, for the Mn-rich compounds, the Fe/Mn($3f$) moments do not actually disappear at T_C, but their size significantly drops to a lower value. With further increasing temperature, the Fe/Mn($3f$) moments gradually decrease and vanish at T_O, while the Mn($3g$) moments prevail above T_O. The evolution of these moments leads to the nonlinear variations of the lattice parameters via the magnetoelastic coupling. Thus, T_O represents the onset of the moment formation on the $3f$ site.

In Fig. 8, the magnetic susceptibility at temperatures above T_C is shown for the $x = 1.25$ sample. In the paramagnetic state, the magnetic susceptibility deviates from the Curie–Weiss law, up to $T^* \sim 630$ K. The paramagnetic Curie temperature (θ_p) is estimated to be about 400 K. The deviation of the susceptibility from the Curie–Weiss law is a general feature for hexagonal Fe_2P-based compounds and is often ascribed to short-range magnetic order.[18–20] We suggest that the decrease

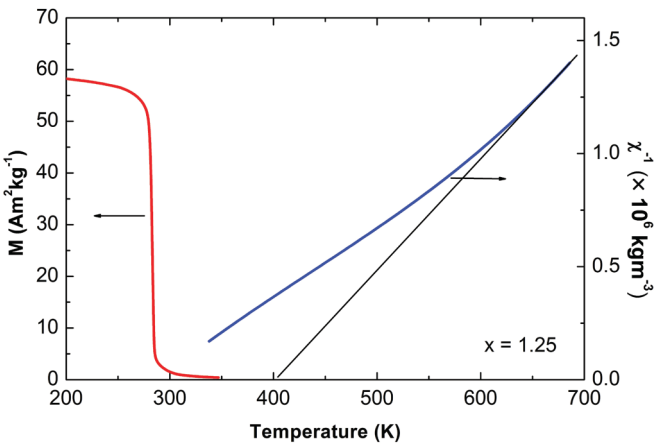

FIG. 8. (Color online) Magnetization and inverse susceptibility as a function of temperature measured in 0.1 T upon heating for $Mn_{1.25}Fe_{0.70}P_{0.50}Si_{0.50}$.

in the magnetic moments upon heating also contributes to the nonlinear variation of the inverse susceptibility at temperatures below T_O. Using the Curie–Weiss law, the effective moment per formula unit (μ_{eff}) can be derived from the Curie constant (C) by:

$$C = \frac{\mu_0 N \mu_{eff}^2}{3k_B}, \quad (1)$$

where C is taken as inverse slope of the χ^{-1}-T curve, N is the number of formula units per mass unit, μ_0 is the magnetic constant, and k_B is the Boltzmann's constant. The Curie–Weiss fit above 630 K leads to a μ_{eff} of about 4.2 μ_B for the $x = 1.25$ sample.

The Rhodes–Wohlfarth ratio q_c/q_s[21,22] is frequently used to distinguish between local moment and itinerant-electron ferromagnetism. Here, q_c and q_s are deduced from the Curie constant and from the low-temperature saturation magnetization, respectively, by using the formulas:

$$\mu_{eff}^2 = N_{at} q_c (q_c + 2) \mu_B^2 \quad (2)$$

and

$$\mu_s = q_s \mu_B, \quad (3)$$

where N_{at} is the number of magnetic atoms per formula unit and μ_s is the average ordered moment per magnetic atom at low temperature. For the $x = 1.25$ sample, the magnetization data and neutron diffraction measurements at 5 K give values for μ_s of 1.9 and 2.1 μ_B, respectively. Assuming magnetic moments on the $3g$ and $3f$ sites, we obtain a q_c of 2.1 from Eq. (2). The ratio q_c/q_s of about 1 seems to give an indication of localized magnetism.[21,22] Our calculation for $MnFeP_{0.85}Ge_{0.15}$ using the data reported by Yabuta *et al.*[20] also leads to the ratio q_c/q_s of 1. These results are in contradiction with the generally agreed description of the hexagonal Fe_2P-based alloys as itinerant-electron magnetic compounds. We propose that this deviation from the Rhodes–Wohlfarth plot may arise from the large difference between the high- and low-moment phases at low and high temperature, respectively (see Fig. 9).

The low-moment phase, which has only magnetic moments on the $3g$ sites, only exists in the paramagnetic state at high temperature. It would become ferromagnetic at the para- to ferromagnetic transition temperature of the low-moment phase (T_C^{LM}) in the vicinity of θ_p. However, the ferromagnetic state of the low-moment phase is apparently not energetically preferred, which indicates that the high-moment phase possesses a lower free energy under the same condition. From the Rhodes–Wohlfarth plot,[21] q_c/q_s of an itinerant-electron ferromagnetic system with $T_C = 400$ K is roughly estimated to be about 1.7. For the $x = 1.25$ sample, since the low-moment phase has T_C^{LM} somewhat lower than 400 K, we may assume that the ratio q_c/q_s of the low-moment phase is 1.7. On the other hand, when we assume for the low-moment phase only magnetic moments on the $3g$ sites, q_c is found to be about 3.3. We therefore deduce $q_s \sim 1.9$, and $\mu_s \sim 1.9\ \mu_B$. This value of μ_s reflects the magnitude of the ordered Mn($3g$) moments of the low-moment phase at low temperature. Hence, the first-order magneto-elastic transition for the $x = 1.25$ sample produces the Fe/Mn($3f$) moments of 1.5 μ_B and the Mn($3g$) moments of 2.6 μ_B.

The following physical picture evolves from our results: At high temperatures above T_O, Mn on the $3g$ sites carries magnetic moments, and the $3f$ sites are predominantly in the bonding state. At lower temperatures, due to ferromagnetic exchange interaction between the Mn($3g$) moments the Fe/Mn($3f$) moments experience a local field that supports the nonbonding high-moment state. Furthermore, it can be seen that magnetic order is enhanced upon cooling. The high-temperature magnetic disorder at $T > T^*$ changes into a short-range magnetic order in the range of $T^* > T > T_C$ before developing into a long-range magnetic order at $T < T_C$ (see Fig. 9). The enhanced magnetic order which gives rise to an increase in the exchange field therefore supports the formation and evolution of the Fe/Mn($3f$) moments. The exchange fields are critical for the moment formation and for the development of ferromagnetic order which occur at T_O and T_C, respectively. The short-range magnetic order therefore plays an important role in the mechanism of the first-order magneto-elastic transition in the hexagonal Mn-Fe-P-Si compounds. An external magnetic field can also support the nonbonding high-moment state and make the transition happen at higher temperatures (see Fig. 10). The value of dT_C/dB is estimated to be about 3.0–3.5 K/T for the $x = 1.25$ sample.

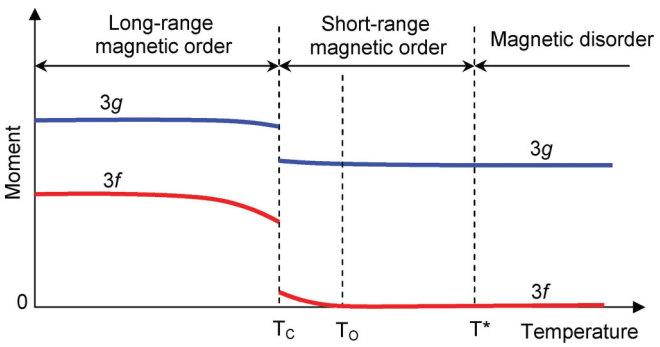

FIG. 9. (Color online) Sketch of the magnetic moments near the first-order magneto-elastic transition in hexagonal Mn-Fe-P-Si compounds. The itinerant moments are not to scale.

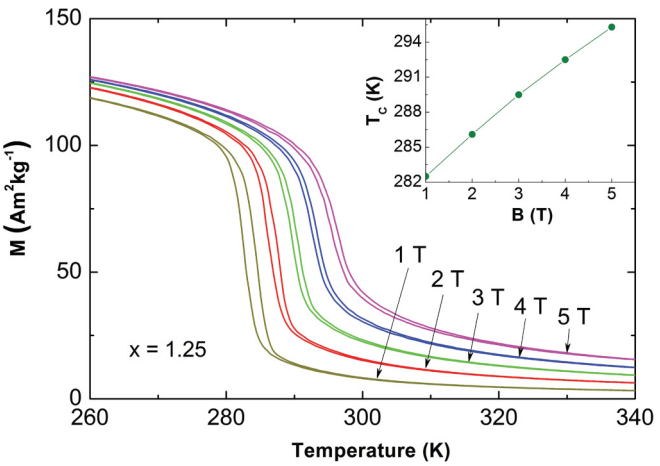

FIG. 10. (Color online) Temperature dependence of the magnetization measured in different magnetic fields (from 1 to 5 T) upon cooling and heating for $Mn_{1.25}Fe_{0.70}P_{0.50}Si_{0.50}$. The inset shows the field dependence of the transition temperature derived from the M-T curves measured upon cooling.

IV. CONCLUSIONS

In summary, a general physical picture of the evolution of the magnetic moments has been put forward for the Mn-rich hexagonal Mn-Fe-P-Si compounds with first-order magneto-elastic transition. The substitution of Mn for Fe on the $3f$ sites does not cause a change in the Mn($3g$) magnetic moments but results in a linear decrease in the magnitude of the Fe/Mn($3f$) magnetic moments. The reduction of the magnetic moments with increasing temperature below the transition temperature has been observed by using neutron diffraction. The sudden change in the interatomic distances validates our description of high/low-moment phase transition, which leads to the deviation from the Rhodes–Wohlfarth plot. The formation and gradual development of the magnetic moment on the $3f$ sites upon cooling give rise to anomalous thermal expansion in the paramagnetic state. By exploiting high-temperature magnetic-susceptibility measurement, we demonstrate the difference of the magnitude of the magnetic moments at low and high temperatures. This paper also reveals the role of short-range magnetic order in the development of the first-order magneto-elastic transition. These results support our proposal that the competition between the moments and chemical bonding is at the core of giant MCE displayed in the class of hexagonal Fe_2P-based materials with first-order magneto-elastic transition.

ACKNOWLEDGMENTS

The authors would like to thank Anton J. E. Lefering, Michel P. Steenvoorde, and Bert Zwart (Delft University of Technology) for their help in magnetic and structural measurements and sample preparation. This work is part of the Industrial Partnership Program I18 of the Dutch Foundation for Fundamental Research on Matter (FOM), and cofinanced by BASF Future Business.

*Corresponding author: h.d.nguyen@tudelft.nl

[1] E. Brück, J. Phys. D Appl. Phys. **38**, R381 (2005).
[2] V. K. Pecharsky and K. A. Gschneidner, Phys. Rev. Lett. **78**, 4494 (1997).
[3] A. Fujita, S. Fujieda, Y. Hasegawa, and K. Fukamichi, Phys. Rev. B **67**, 104416 (2003).
[4] N. T. Trung, L. Zhang, L. Caron, K. H. J. Buschow, and E. Brück, Appl. Phys. Lett. **96**, 172504 (2010).
[5] T. Krenke, E. Duman, M. Acet, E. F. Wassermann, X. Moya, L. Manosa, and A. Planes, Nat. Mater. **4**, 450 (2005).
[6] O. Tegus, E. Brück, K. H. J. Buschow, and F. R. de Boer, Nature **415**, 150 (2002).
[7] N. H. Dung, Z. Q. Ou, L. Caron, L. Zhang, D. T. C. Thanh, G. A. de Wijs, R. A. de Groot, K. H. J. Buschow, and E. Brück, Adv. Energy Mater. **1**, 1215 (2011).
[8] D. Haskel, Y. B. Lee, B. N. Harmon, Z. Islam, J. C. Lang, G. Srajer, Y. Mudryk, K. A. Gschneidner, and V. K. Pecharsky, Phys. Rev. Lett. **98**, 247205 (2007).
[9] M. D. Kuz'min and M. Richter, Phys. Rev. B **76**, 092401 (2007).
[10] J. Lyubina, K. Nenkov, L. Schultz, and O. Gutfleisch, Phys. Rev. Lett. **101**, 177203 (2008).
[11] N. H. Dung, L. Zhang, Z. Q. Ou, and E. Brück, Appl. Phys. Lett. **99**, 092511 (2011).
[12] K. D. Liss, B. Hunter, M. Hagen, T. Noakes, and S. Kennedy, Physica B **385-386**, 1010 (2006).
[13] A. W. Hewat, Mater. Sci. Forum **9**, 69 (1986).
[14] J. Rodriguez-Carvajal, Physica B **192**, 55 (1993).
[15] V. Hoglin, M. Hudl, M. Sahlberg, P. Nordblad, P. Beran, and Y. Andersson, J. Solid State Chem. **184**, 2434 (2011).
[16] L. Zhang, O. Moze, K. Prokes, O. Tegus, and E. Brück, J. Magn. Magn. Mater. **290**, 679 (2005).
[17] D. M. Liu, Q. Z. Huang, M. Yue, J. W. Lynn, L. J. Liu, Y. Chen, Z. H. Wu, and J. X. Zhang, Phys. Rev. B **80**, 174415 (2009).
[18] O. Beckman and L. Lundgren, in *Handbook of Magnetic Materials*, edited by K. H. J. Buschow (Elsevier, Amsterdam, 1991), Vol. 6, pp. 181.
[19] R. Zach, M. Guillot, and R. Fruchart, J. Magn. Magn. Mater. **89**, 221 (1990).
[20] H. Yabuta, K. Umeo, T. Takabatake, K. Koyama, and K. Watanabe, J. Phys. Soc. Jpn. **75**, 113707 (2006).
[21] P. Rhodes and E. P. Wohlfarth, Proc. R. Soc. A **273**, 247 (1963).
[22] E. P. Wohlfarth, J. Magn. Magn. Mater. **7**, 113 (1978).